Nonvolatile Ferroelectric Field Control of the Anomalous Hall Effect in $BiFeO_3/SrRuO_3$ Bilayer

Z.Y. Ren, F. Shao, P.F. Liu, M.X. Wang, J.K. Chen, K.K. Meng, X.G. Xu, J. Miao,* and Y. Jiang†
Beijing Advanced Innovation Center for Materials Genome Engineering, School of Materials Science and Engineering, University of Science and Technology Beijing, Beijing 100083, China

(Received 16 October 2019; revised manuscript received 15 December 2019; accepted 30 January 2020; published 18 February 2020)

Here, the $BiFeO_3/SrRuO_3$ heterostructure is fabricated and the anomalous Hall effect (AHE) is investigated. The nonmonotonic anomalous Hall resistivity behavior in $BiFeO_3/SrRuO_3$ originates from the inhomogeneous $SrRuO_3$ layer instead of the topological Hall effect. It is surprising that the AHE in the $BiFeO_3/SrRuO_3$ structure can be manipulated by switching the ferroelectric polarization of $BiFeO_3$. Furthermore, the modulation of AHE in $SrRuO_3$ under ferroelectric polarization is discussed with respect to first-principles calculations and originates from the change of band structure around the Fermi level. The ferroelectric-manipulated AHE suggests a pathway to realize nonvolatile, reversible, and low-energy-consuming voltage-controlled spintronic devices.

DOI: 10.1103/PhysRevApplied.13.024044

I. INTRODUCTION

In the past decade, electric-field control of spin transport has attracted intensive attention and provided the potential to reduce power consumption for spintronic devices, such as memory and logic devices [1,2]. Several interesting physical mechanisms in electric-field control of spin transport are reported, including interfacial strain or stress coupling [3,4], redox reactions at the metal-oxide interface [5,6], and the accumulation of spin current [7]. Multiferroic heterostructures, consisting of ferroelectric and ferromagnetic layers, have significant advantages in electric-field control of spin-transporting behavior. The magnetoelectric coupling strength of multiferroic heterostructures is much larger than that of single-phase multiferroic materials [8]. Compared with GdO_x [9], Al_2O_3 [10] multiferroic heterostructures can result in high-speed performance, low voltage, and nonvolatile devices [11,12].

$SrRuO_3$ is a type of complex oxide perovskite with itinerant ferromagnetism, which has fascinating properties originating from the strong spin-orbit coupling. The anomalous Hall effect (AHE) in $SrRuO_3$ is related to the Berry curvature, which implies that the Hall conductivity σ_{xy} depends critically on band-structure details of material magnetization, and particularly on band crossings around the Fermi level [13–15]. Moreover, the temperature dependence of Hall resistivity in $SrRuO_3$ is not only nonmonotonic, but also changeable in the sign of AHE at a critical temperature [16,17]; this is closely related to temperature-dependent band crossings [18]. Most interestingly, the topological Hall effect (THE) has been observed in perovskite heterostructures $SrRuO_3/SrIrO_3$ [19,20] and $SrRuO_3/BaTiO_3$ [21], and then attributed to the formation of skyrmions because a strong Dzyaloshinskii-Moriya interaction can occur on artificial interfaces, hosting topologically nontrivial spin textures in $SrRuO_3$. Although the exact mechanism of the AHE and the presence of THE in $SrRuO_3$ remain debatable, the electron distributions around the Fermi energy surely play an important role in $SrRuO_3$. Here, we show that electron distributions around the Fermi energy in $SrRuO_3$ can be affected by ferroelectric polarization.

Here, we report that the nonmonotonic anomalous Hall resistivity (R_{AHE}) behavior in $BiFeO_3/SrRuO_3$ originates from the inhomogeneous $SrRuO_3$ layer instead of the THE. Furthermore, the polarization-field-induced effects on the AHE of the $BiFeO_3/SrRuO_3$ heterostructure are realized and both the magnitude and sign of R_{AHE} can be modulated by manipulating the polarization of $BiFeO_3$. $BiFeO_3$ is a multiferroic material that can provide a remanent ferroelectric field; this is nonvolatile and modulates $SrRuO_3$. Moreover, with only one low-voltage pulse, we can switch the polarization of $BiFeO_3$, so modulation of the AHE by polarization is reversible and consumes little energy. The nonvolatile modulation of the AHE originates from the change in the band structure around the Fermi level in $SrRuO_3$ under ferroelectric polarization, which is explored by first-principles calculations. Therefore, the ferroelectric-manipulated AHE suggests a pathway to study spin transport in multiferroic heterostructures.

*j.miao@ustb.edu.cn
†yjiang@ustb.edu.cn

II. EXPERIMENT

Samples of $La_{0.7}Sr_{0.3}MnO_3$(10 nm)/$BiFeO_3$(100 nm)/$SrRuO_3$(20 nm) are epitaxially grown on $SrTiO_3$(001) substrates using pulsed laser deposition (PLD); $La_{0.7}Sr_{0.3}MnO_3$ (10 nm) is used as a bottom electrode for the $La_{0.7}Sr_{0.3}MnO_3/BiFeO_3/SrRuO_3$ structure. Films of $SrRuO_3$ and $BiFeO_3$ are grown by PLD using a KrF laser with a fluence around 1.5 and 1.0 J/cm^2, respectively, and a repetition rate of 3 Hz. Before deposition, the base pressure of the chamber is less than 1×10^{-4} Pa, while during deposition the oxygen partial pressure is 10 Pa and the temperature is 780 °C. To obtain the high-quality film, after deposition, the oxygen pressure is kept at 10^4 Pa and then the films are cooled to room temperature.

Figure 1(a) shows the x-ray diffraction (XRD) ω-2θ scan pattern for the $La_{0.7}Sr_{0.3}MnO_3/BiFeO_3/SrRuO_3$ sample, which determines the phase structure of the $La_{0.7}Sr_{0.3}MnO_3$, $SrRuO_3$, and $BiFeO_3$ films. $La_{0.7}Sr_{0.3}MnO_3$ (00l), $SrRuO_3$ (00l), and $BiFeO_3$ (00l) peaks can be observed clearly, which demonstrates the uniaxial orientation growth of $La_{0.7}Sr_{0.3}MnO_3$, $SrRuO_3$, and $BiFeO_3$. A topographic image of $La_{0.7}Sr_{0.3}MnO_3/BiFeO_3/SrRuO_3$ is obtained by atomic force microscopy (AFM), as shown in Fig. 1(b). The scan area is 1×1 μm^2, and the root-mean-square roughness is 0.38 nm for $La_{0.7}Sr_{0.3}MnO_3/BiFeO_3/SrRuO_3$, which means that the film surfaces are atomically flat. The experimental geometry Hall bar is shown in Fig. 1(c), and the Hall bar is prepared by electron beam lithography and Ar^+ etching, with a size of 20×20 μm^2. The resistance measurements are performed via a physical property measurement system (PPMS) and the channel current, I, along the x axis is constantly 100 μA.

III. RESULTS AND DISCUSSION

A. Anomalous Hall effect in the $BiFeO_3/SrRuO_3$ bilayer

Figure 1(d) shows the current-voltage (I-V) characteristics of the $La_{0.7}Sr_{0.3}MnO_3/BiFeO_3/SrRuO_3$ trilayers at 80 K. The I-V curve shows that the leakage current is low, which means $BiFeO_3$ is high quality and insulated. In Fig. 2(b), the temperature dependence of the longitudinal resistivity (R_{xx}) is shown; the resistivity of $SrRuO_3$ decreases as the temperature decreases, which indicates a metallic property. It also indicates that the Curie temperature (T_C) in our $SrRuO_3$ film (approximately 125 K) is lower than that of the $SrRuO_3$ bulk value (approximately 160 K) [22], which is consistent with the previously reported value in $SrRuO_3$ films (approximately 130 K) [23]. It is noteworthy that the current, which is only through $SrRuO_3$, is verified by the leakage mechanism. The Hall resistance (R_{xy}) is measured by sweeping the magnetic field, H, perpendicular to the sample's surface, the magnetic field is from –3 to 3 T, and the temperature is from 50 to 120 K. The ρ_{xy} value can be expressed

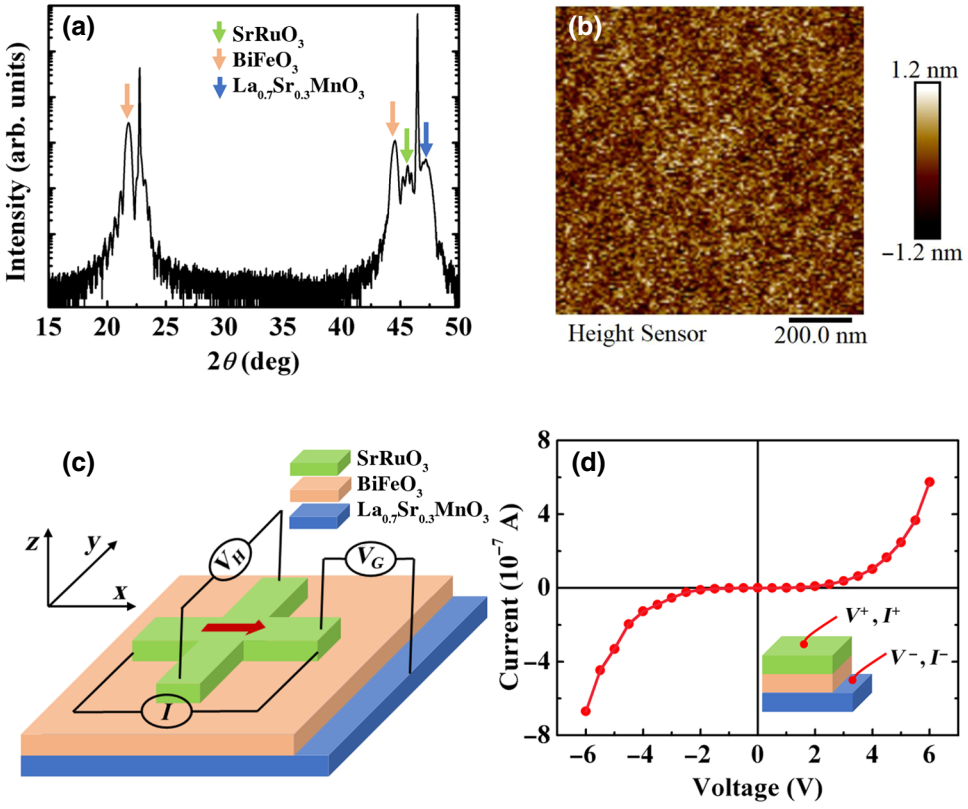

FIG. 1. (a) XRD pattern and (b) AFM image of the $SrTiO_3$/$La_{0.7}Sr_{0.3}MnO_3$(10 nm)/$BiFeO_3$(100 nm)/$SrRuO_3$(20 nm) sample. (c) Schematic diagram of the Hall bar structure. (d) I-V curves for $La_{0.7}Sr_{0.3}MnO_3$(10 nm)/$BiFeO_3$(100 nm)/$SrRuO_3$(20 nm) at 80 K.

as $\rho_{xy} = \rho_{OHE} + \rho_{AHE}$, where the two terms denote the ordinary and anomalous Hall resistivities, respectively [24]. The ordinary Hall effect (OHE) is described by $\rho_{OHE} = R_0 H$, where R_0 and H are the ordinary Hall coefficient and out-of-plane magnetic field, respectively. The AHE is described by $\rho_{AHE} = R_S M$, where R_S and M are the anomalous Hall coefficient and out-of-plane magnetic moment, respectively. To evaluate ρ_{AHE}, ρ_{OHE} should be extracted, and thus, the ordinary part, by linearly fitting ρ_{xy}, can be determined in the higher magnetic-field region.

Figure 2(a) shows the magnetic-field dependence of R_{AHE} in the $SrRuO_3$ channel from 50 to 120 K. The curves exhibit a square-shaped hysteresis, which indicates the H-induced reversal of magnetization, confirming that magnetization of the $SrRuO_3$ layer has good perpendicular magnetic anisotropy (PMA). It is found that the R_{AHE}-H curves show humps from 80 to 100 K. Recently, a similar nonmonotonic R_{AHE}-H behavior was reported in $SrIrO_3/SrRuO_3$ bilayer [19,20] and $BaTiO_3/SrRuO_3$ bilayer [21] skyrmion systems, and it was clarified that these humps should be assigned to the THE. In a prototypical magnetic skyrmion system, the transverse Hall resistivity, ρ_{xy}, can be decomposed into three terms, $\rho_{xy} = \rho_{OHE} + \rho_{AHE} + \rho_{THE}$, where ρ_{THE} is the topological Hall resistivity [19]. However, in $(Bi, Mn)_2Se_3$ thin film [25], the positive and negative anomalous Hall resistances are found to coexist, and the Hall resistivity of $(Bi, Mn)_2Se_3$ shows a peak and valley. As reported by Gerber [26], the distinct nonmonotonic features in the Hall effect signal arise in heterogeneous ferromagnets, when components of the material exhibit the AHE with opposite polarities. Also, Kan *et al.* [27] reported the THE-like signal in $SrRuO_3$, arising from the inhomogeneous magnetoelectric properties of $SrRuO_3$. Thus, the origin of the AHE in $SrRuO_3$ may still be debated.

To clarify the origin of the hump in the $SrRuO_3/BiFeO_3$ heterostructure, we define R_{hump} as the height of the hump with respect to the saturation resistivity. Figures 2(c) and 2(d) summarize the temperature dependence of R_{AHE}, R_{hump}, and coercive field (H_C). As shown in Fig. 2(c), the sign of R_{AHE} changes from negative to positive at $T_S \sim 85$ K, where T_S is the transition temperature at which the sign of R_{AHE} reverses. This change of R_S is also confirmed from the temperature dependence of the anomalous Hall conductivity, σ_{AHE}, in $SrRuO_3$, and the sign change of R_S may be attributed to the Berry curvature [18]. Also, R_{hump} shows a peak around T_S. As shown in Fig. 2(d), H_C decreases with decreasing temperature and exhibits a discontinuity around T_S. This indicates that all abnormalities are related to reversal of the sign of R_{AHE} in $SrRuO_3$.

As shown in Fig. 2(e), the field sweeps from +1.5 T to negative maximum field (Hn_{max}), and then back to the +1.5 T. When $|Hn_{max}| < 0.2$ T, only domains with positive AHE can be switched, so the humps vanish. When $|Hn_{max}| > 0.2$ T, the domains with negative AHE can be switched, and thus, the humps emerge. The emergence

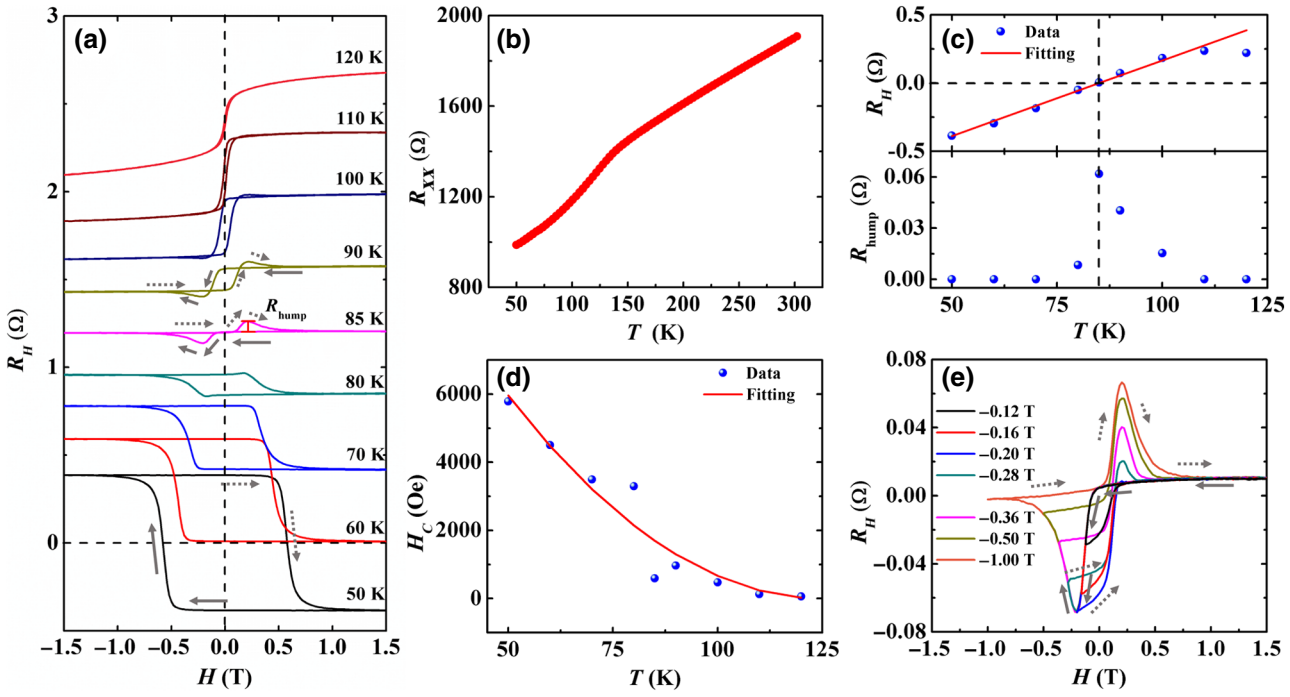

FIG. 2. (a) Magnetic-field dependence of R_{AHE} at different temperatures. (b) R_{xx}, (c) R_{AHE} and R_{hump}, and (d) H_C as a function of temperature. (e) Minor loops of R_{AHE} at 85 K for $BiFeO_3/SrRuO_3$. Temperature dependence of R_{AHE} and H_C are fitted by linear and quadratic functions, respectively (red line). The arrow represents the magnetic-field sweep direction.

of humps and R_{hump} in the positive field depends on Hn_{max}, which indicates that the $SrRuO_3$ film is inhomogeneous, with domains with different $H_C(T)$ and $R_{AHE}(T)$ [27,28]. Therefore, the nonmonotonic R_{AHE}-H behavior in $BiFeO_3/SrRuO_3$ arises from inhomogeneous $SrRuO_3$. The inhomogeneity may arise from asymmetric boundary conditions [28], inhomogeneous thickness [29], oxygen octahedral rotation [30,31], and the ferroelectric proximity effect [32]. The ferroelectric proximity effect induced inhomogeneity can be modulated by manipulating the ferroelectric field of $BiFeO_3$.

B. Ferroelectric polarization control of the anomalous Hall effect

Next, the ferroelectric-manipulated AHE in $BiFeO_3/SrRuO_3$ heterostructures are demonstrated. Ferroelectric properties of the $BiFeO_3$ film are investigated using piezoresponse force microscopy (PFM) at room temperature. Figure 3(a) shows the PFM image of $La_{0.7}Sr_{0.3}MnO_3/BiFeO_3$ as the initial state. Figures 3(b) and 3(c) show the phase and amplitude of the $BiFeO_3$ layer with upward and downward polarization under −9 and +9 V, respectively. The PFM indicates that the polarization of $BiFeO_3$ in the initial state is upward, which is consistent with a previous report [33]. Besides, a clear hysteretic behavior in $La_{0.7}Sr_{0.3}MnO_3/BiFeO_3$ is observed in both phase and magnitude of the signal in Fig. 3(d). These results clearly show the good ferroelectric properties of $BiFeO_3$.

As shown in Fig. 4(a), the impulse gate voltage with ±9 V (downward-upward polarization of $BiFeO_3$) in the Hall bar is applied in situ by using a Keithley 4200 instrument, then the gate voltage is removed and R_{AHE}-H is measured. Figures 4(b)–4(e) show the R_{AHE}-H curves of the initial state, oppositely switched state, and reversibly switched state for the heterostructures, at 80, 85, 90, and 100 K, respectively. It is noted that the as-grown ferroelectric polarization is upward. Furthermore, when ferroelectric polarization is from upward to downward, the shapes of the R_{AHE}-H curves change and the decrease of R_{AHE} are clearly observed. Moreover, when ferroelectric polarization is switched back to the original state, the shapes of the R_{AHE}-H curves are indeed switched back to the initial state. It should be noted that the voltage is removed during the measurement. Thus, the current-induced heating is negligible. The heating effect will be symmetrical in the R_{AHE}-H variation with respect to the applied voltage. Notably, R_{AHE}-H is different for +9 and –9 V, but primarily the same for –9 V and the as-grown state. Thus, the mock effect induced by Joule heating can be ruled out. Similarly, the strain effect in the $SrRuO_3/BiFeO_3$ heterostructure can also be excluded, since the piezoelectricity in $BiFeO_3$ is small and ferroelastic effects would give an even contribution. These results confirm that the AHE in $SrRuO_3$ can be modulated by the ferroelectric remanent polarization in $BiFeO_3$ along the out-of-plane direction. In particular, this modulation effect on AHE in $SrRuO_3/BiFeO_3$ is nonvolatile and reversible.

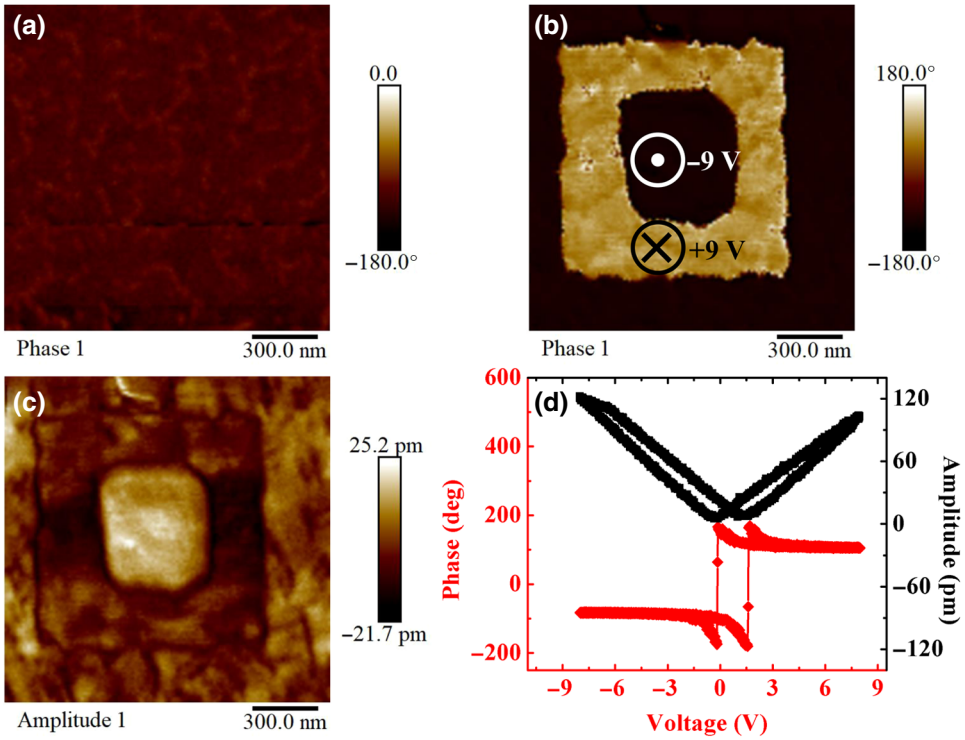

FIG. 3. PFM images of the $SrTiO_3/La_{0.7}Sr_{0.3}MnO_3$(10 nm)/$BiFeO_3$(100 nm) structure: (a) initial phase and (b) phase and (c) amplitude after writing under ±9 V, respectively. (d) Ferroelectric-phase hysteresis and strain loops.

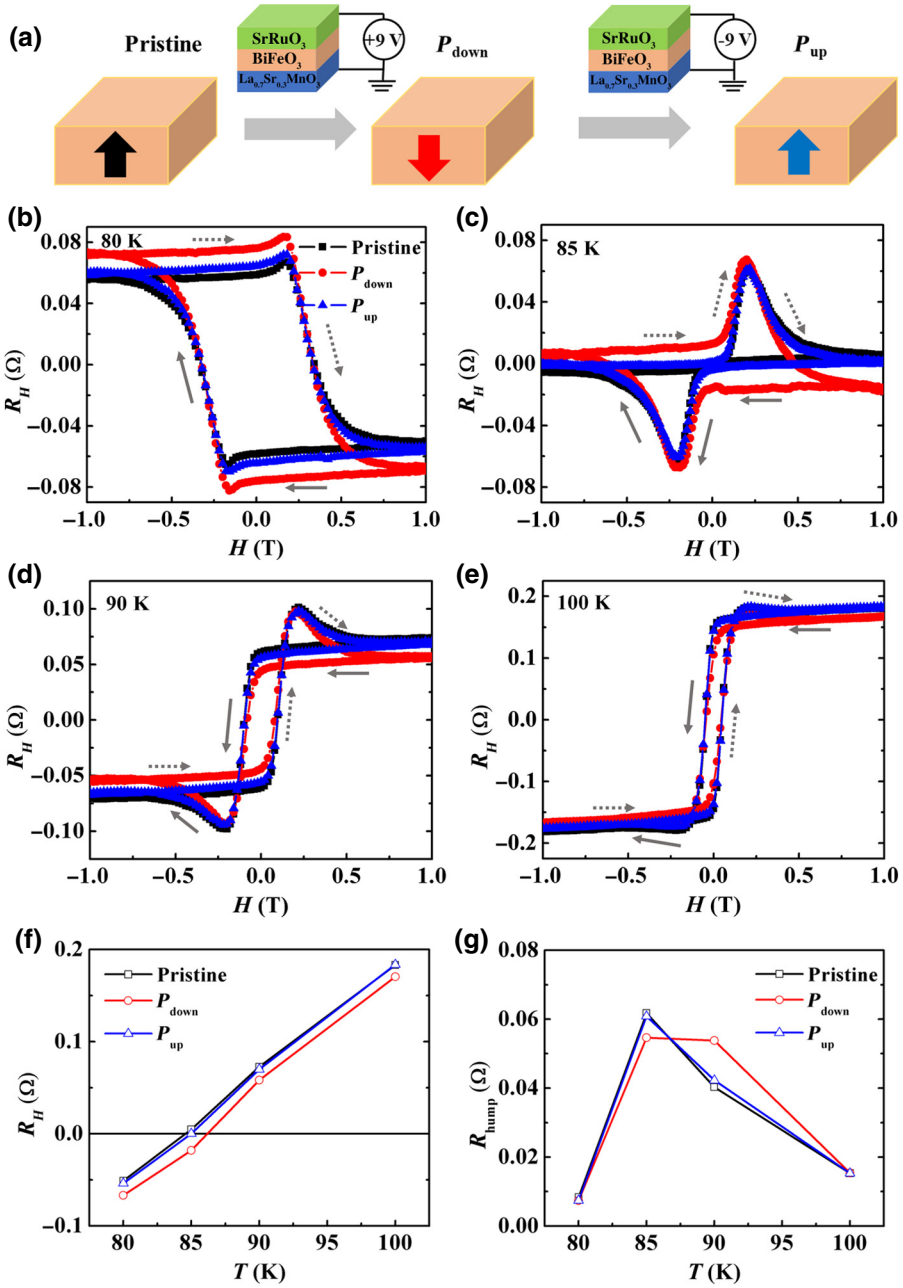

FIG. 4. (a) In $BiFeO_3/SrRuO_3$ heterostructure, the ferroelectric polarization as-grown is upward, with +9 V is downward, and with −9 V is upward. R_{AHE}-H hysteresis loops of $BiFeO_3/SrRuO_3$ heterostructure in as-grown state, oppositely switched state, and reversibly switched state at (b) 80 K, (c) 85 K, (d) 90 K, and (e) 100 K. The arrows show the direction of polarization. (f) R_{AHE} and (g) R_{hump} as a function of temperature under as-grown state, oppositely switched state, and reversibly switched state.

To clearly observe the ferroelectric-manipulated AHE in $La_{0.7}Sr_{0.3}MnO_3/BiFeO_3/SrRuO_3$ heterostructures, we summarize the temperature dependence of R_{AHE} and R_{hump}. As shown in Fig. 4(f), a vertical translation of R_{AHE} in $R_{AHE}(T)$ between the upward and downward polarization can be observed. It is interesting to note that the ferroelectric polarization modulation can give rise to the sign inversion of R_{AHE}. As shown in Fig. 4(g), first, R_{hump} of upward polarization is larger than that of downward polarization, then R_{hump} of upward polarization is smaller than that of downward polarization, indicating a horizontal translation of R_{hump} in $R_{hump}(T)$ between the two ferroelectric polarization states. The vertical translation of R_{AHE} and the horizontal translation of R_{hump} indicate that T_S values in $SrRuO_3/BiFeO_3$ are 85 K and 86.5 K for the upward and downward polarization, respectively. Notably, $R_{AHE}(T)$ [$R_{hump}(T)$] with upward polarization and the as-grown state are approximately same.

Here, modulation depends on the remanent ferroelectric polarization of $BiFeO_3$, and thus, modulation can be realized by a low impulse voltage. Nonvolatile and low energy consumption characteristics are important for a voltage-controlled device. As shown in Fig. 5, the AHE under ferroelectric polarization of the $BiFeO_3$ layer is repeatedly poled upward and downward at 85 K. Thus, the ferroelectric polarization-manipulated AHE is reversible and nonvolatile.

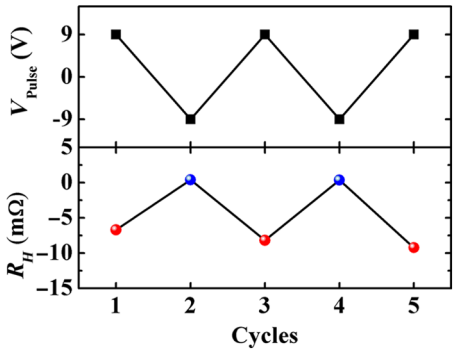

FIG. 5. Polarization of the $BiFeO_3$ layer is repeatedly poled upward and downward, with R_{AHE} under upward and downward polarization, respectively.

Now, we are trying to understand the mechanism of the ferroelectric-manipulated AHE in $BiFeO_3/SrRuO_3$ heterostructures. According to the formulation of a model considering inhomogeneous magnetoelectric properties in $SrRuO_3$ [27], the ferroelectric-manipulated R_{AHE}-H curves can be completely reproduced.

$$f(T', H) = \rho_H(T')\{1 - 2H_{Heav}[H - H_C(T')]\}g(T'). \quad (1)$$

As described in Eq. (1), each domain contributes an effective field response to the transverse resistivity. As shown in Figs. 2(c) and 2(d), $R_{AHE}(T')$ and $H_C(T')$ are the actual temperature dependence of R_{AHE} and H_C, respectively, which are fitted by linear and quadratic functions, respectively: $R_{AHE}(T') = -0.94062 + 0.01106T'$ and $H_C(T') = 1.0597(T'-125)^2$. The magnetic moment reversal is described by the Heaviside step function, $H_{Heav}(x)$, and $g(T')$ is the Gaussian function describing a distribution of the domain as

$$g(T') = \frac{1}{\sqrt{2\pi T_\sigma^2}} \exp\left[\frac{(T'-T)^2}{2T_\sigma^2}\right], \quad (2)$$

$$\Gamma(H) = \int_0^\infty f(T')dT'. \quad (3)$$

In Figs. 6(a) and 6(b), calculations of the R_{AHE}-H loops by integrating Eq. (3) for upward and downward state are shown, respectively. Both of them are well reproduced in experiments, indicating that the R_{AHE}-H nonmonotonic behavior in $BiFeO_3/SrRuO_3$ arises from the inhomogeneity of $SrRuO_3$ film. As shown in Figs. 6(c) and 6(d), the temperature dependence of R_{AHE} and R_{hump} is extracted from the calculated loops. These data show a vertical translation of R_{AHE} in $R_{AHE}(T)$ and a horizontal translation of R_{hump} in $R_{hump}(T)$ between the two ferroelectric polarization states, which are consistent with experiments of $R_{AHE}(T)$ and $R_{hump}(T)$ in $BiFeO_3/SrRuO_3$ under the upward and downward polarization.

Neither the skew-scattering theory nor the side-jump theory seem to be adequate to explain the origin of the AHE in $SrRuO_3$ layer [18]. Recently, the Berry-phase theory is applied to account for it [18,34]. The first-principles calculations show that the AHE conductivity fluctuates strongly with the variation of energy, which is related to the Berry curvature. Therefore, in this work, modulation of the AHE in $SrRuO_3$ may be related to the change of Berry curvature. To further account for the microscopic nature of the ferroelectric-manipulated AHE in $BiFeO_3/SrRuO_3$ heterostructures, the electronic structure of $SrRuO_3$ is calculated using the first-principles calculation. The calculations are performed for the $SrRuO_3$ using the Vienna ab

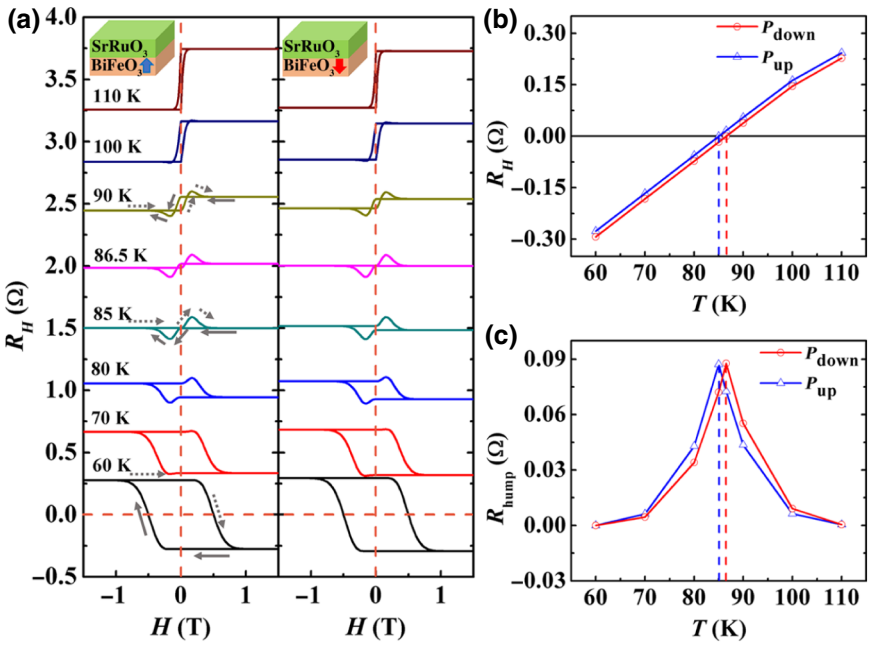

FIG. 6. R_{AHE}-H hysteresis loops reproduced by a numerical model with (a) upward and (b) downward polarization in $BiFeO_3/SrRuO_3$. Temperature dependence of calculated (c) R_{AHE} and (d) R_{hump} with upward and downward.

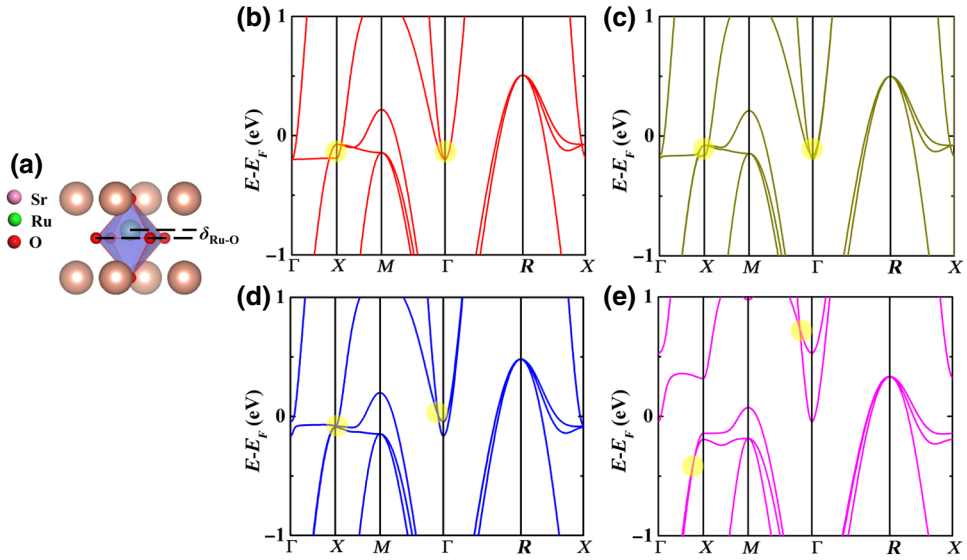

FIG. 7. (a) Schematic diagram of $SrRuO_3$; the ionic displacement between oxygen and Ru along the [001] axis is denoted as $\delta_{Ru—O}$. The band structure of $SrRuO_3$ with $\delta_{Ru—O}$ as (b) 0.00 c, (c) 0.01 c, (d) 0.02 c, and (e) 0.05 c.

initio simulation package (VASP) with generalized gradient approximation [35]. The cutoff energy for the plane-wave basis set is 500 eV. We set the three-dimensional Brillouin zone (BZ) as $9 \times 9 \times 9$ k mesh for the primitive cell of $SrRuO_3$ and the spin-orbit coupling is included in all calculations. As shown in Fig. 7(a), we assume that Ru and O diverge, as described by $\delta_{Ru—O}$ on the basis of the ferroelectric proximity effect [21,36–38]. The band structures of $SrRuO_3$ with $\delta_{Ru—O} = 0$ c, 0.01 c, 0.02 c, and 0.05 c are shown in Figs. 7(b)–7(e), respectively; $c = 3.99$ Å is the lattice constant of $SrRuO_3$. It is found that the band structures of $SrRuO_3$ show the difference near the Fermi energy under different $\delta_{Ru—O}$. The Berry curvature is determined by the band structure near the Fermi energy, and the anomalous Hall conductivity is proportional to the integral of Berry curvature. The change of crossing points around Γ and X can provide a prominent contribution to the AHE [39]. Furthermore, $\delta_{Ru—O}$ gradually decreases from the heterointerface to the interior of $SrRuO_3$, which can give rise to inhomogeneous $SrRuO_3$ [21]. Moreover, $|\delta_{Ru—O}|$ under the upward and downward polarization are always different [21,32,36], and thus, the AHE and Berry curvature under the opposite ferroelectric polarization direction are different.

IV. CONCLUSIONS

The AHE in $BiFeO_3/SrRuO_3$ heterostructure is investigated. Nonmonotonic R_{AHE}-H in $BiFeO_3/SrRuO_3$ is unrelated to the THE, which originates from the inhomogeneous crystal structure induced by the ferroelectric field and inhomogeneous thickness of the $SrRuO_3$ layer. Besides, nonmonotonic R_{AHE}-H in $BiFeO_3/SrRuO_3$ can be well explained by the inhomogeneous phenomenological model. Furthermore, the AHE in $BiFeO_3/SrRuO_3$ can be manipulated by switching the ferroelectric polarization of $BiFeO_3$. That is, the upward and downward polarization fields of $BiFeO_3$ can increase and decrease the anomalous Hall resistivity, respectively. Moreover, the ferroelectric polarization-manipulated AHE is reversible and nonvolatile. The first-principles calculations show that the modulation of the AHE may be attributed to a change in the electron distributions around the Fermi energy in $SrRuO_3$ with the opposite ferroelectric polarization of $BiFeO_3$. The ferroelectric-manipulated AHE suggests a pathway to realize nonvolatile, reversible, and low-energy-consuming voltage-controlled spintronic devices.

ACKNOWLEDGMENTS

The authors wish to thank Professor Zhe Yuan (Beijing Normal University) and Dr. LingFei Wang (Seoul National University) for fruitful discussions and support. This work is partially supported by the National Key R&D Program of China (Grant No. 2018YFB0704100), the National Science Foundation of China (Grants No. 11974042, No. 51731003, No. 51927802, No. 51971023, No. 11574027, and No. 61674013).

[1] M. Y. Yang, Y. C. Deng, Z. H. Wu, K. M. Cai, K. W. Edmonds, Y. C. Li, Y. Sheng, S. M. Wang, Y. Cui, J. Luo, Y. Ji, H. Z. Zheng, and K. Y. Wang, Spin logic devices via electric field controlled magnetization reversal by spin-orbit torque, IEEE Electron Device Lett. **40**, 1554 (2019).

[2] S. Fusil, V. Garcia, A. Barthelemy, and M. Bibes, Magnetoelectric devices for spintronics, Annu. Rev. Mater. Res. **44**, 91 (2014).

[3] S. Zhang *et al.*, Electric-field Control of Nonvolatile Magnetization in $Co_{40}Fe_{40}B_{20}$/Pb-$(Mg_{1/3}Nb_{2/3})_{0.7}Ti_{0.3}O_3$ Structure at Room Temperature, Phys. Rev. Lett. **108**, 137203 (2012).

[4] L. You, B. Wang, X. Zou, Z. S. Lim, Y. Zhou, H. Ding, L. Chen, and J. L. Wang, Origin of the uniaxial magnetic anisotropy in $La_{0.7}Sr_{0.3}MnO_3$ on stripe-domain $BiFeO_3$, Phys. Rev. B **88**, 184426 (2013).

[5] C. Bi, Y. H. Liu, T. Newhouse-Illige, M. Xu, M. Rosales, J. W. Freeland, O. Mryasov, S. F. Zhang, S. G. E. te Velthuis, and W. G. Wang, Reversible Control of Co Magnetism by Voltage-Induced Oxidation, Phys. Rev. Lett. **113**, 267202 (2014).

[6] H. B. Li, N. P. Lu, Q. H. Zhang, Y. J. Wang, D. Q. Feng, T. Z. Chen, S. Z. Yang, Z. Duan, Z. L. Li, Y. J. Shi, W. C. Wang, W. H. Wang, K. Jin, H. Liu, J. Ma, L. Gu, C. W. Nan, and P. Yu, Electric-field control of ferromagnetism through oxygen ion gating, Nat. Commun. **8**, 2156 (2017).

[7] K. M. Cai, M. Y. Yang, H. L. Ju, S. M. Wang, Y. Ji, B. H. Li, K. W. Edmonds, Y. Sheng, B. Zhang, N. Zhang, S. Liu, H. Z. Zheng, and K. Y. Wang, Electric field control of deterministic current-induced magnetization switching in a hybrid ferromagnetic/ferroelectric structure, Nat. Mater. **16**, 712 (2017).

[8] C. A. F. Vaz and U. Staub, Artificial multiferroic heterostructures, J. Mater. Chem. C. **1**, 6731 (2013).

[9] U. Bauer, L. D. Yao, A. J. Tan, P. Agrawal, S. Emori, H. L. Tuller, S. V. Dijken, and G. S. D. Beach, Magneto-ionic control of interfacial magnetism, Nat. Mater. **14**, 174 (2015).

[10] T. Maruyama, Y. Shiota, T. Nozaki, K. Ohta, N. Toda, M. Mizuguchi, A. A. Tulapurkar, T. Shinjo, M. Shiraishi, S. Mizukami, Y. Ando, and Y. Suzuki, Large voltage-induced magnetic anisotropy change in a few atomic layers of iron, Nat. Nanotechnol. **4**, 1582009 (2009).

[11] P. V. Lukashev, J. D. Burton, S. S. Jaswal, and E. Y. Tsymbal, Ferroelectric control of the magnetocrystalline anisotropy of the $Fe/BaTiO_3(001)$ interface, J. Phys.: Condens. Matter. **24**, 226003 (2012).

[12] C. G. Duan, J. P. Velev, R. F. Sabirianov, W. N. Mei, S. S. Jaswal, and E. Y. Tsymbal, Tailoring magnetic anisotropy at the ferromagnetic/ferroelectric interface, Appl. Phys. Lett. **92**, 122905 (2008).

[13] R. Mathieu, C. U. Jung, H. Yamada, A. Asamitsu, M. Kawasaki, and Y. Tokura, Determination of the intrinsic anomalous Hall effect of $SrRuO_3$, Phys. Rev. B **72**, 064436 (2005).

[14] Y. G. Yao, L. Kleinman, A. H. MacDonald, J. Sinova, T. Jungwirth, D. S. Wang, E. Wang, and Q. Niu, First Principles Calculation of Anomalous Hall Conductivity in Ferromagnetic bcc Fe, Phys. Rev. Lett. **92**, 037204 (2004).

[15] R. Karplus and J. M. Luttinger, Hall effect in ferromagnetics, Phys. Rev. **95**, 1154 (1952).

[16] M. Izumi, K. Nakazawa, Y. Bando, Y. Yoneda, and H. Terauchi, Magnetotransport of $SrRuO_3$ thin film on $SrTiO_3$ (001), J. Phys. Soc. Jpn. **66**, 3893 (1997).

[17] L. Klein, J. R. Reiner, T. H. Geballe, M. R. Beasley, and A. Kapitulnik, Extraordinary Hall effect in $SrRuO_3$, Phys. Rev. B **61**, R7842 (2000).

[18] Z. Fang, N. Nagaosa, K. S. Takahashi, A. Asamitsu, R. Mathieu, T. Ogasawara, T. Ogasawara, H. Yamada, M. Kawasaki, Y. Tokura, and K. Terakura, The anomalous Hall effect and magnetic monopoles in momentum space, Science **302**, 92 (2003).

[19] J. Matsuno, N. Ogawa, K. Yasuda, F. Kagawa, W. Koshibae, N. Nagaosa, Y. Tokura, and M. Kawasaki, Interface-driven topological Hall effect in $SrRuO_3$-$SrIrO_3$ bilayer, Sci. Adv. **2**, e1600304 (2016).

[20] Y. Ohuchi, J. Matsuno, N. Ogawa, Y. Kozuka, M. Uchida, Y. Tokura, and M. Kawasaki, Electric-field control of anomalous and topological Hall effects in oxide bilayer thin films, Nat. Commun. **9**, 213 (2018).

[21] L. F. Wang, Q. Y. Feng, Y. Kim, R. Kim, K. H. Lee, S. D. Pollard, Y. J. Shin, H. B. Zhou, W. Peng, D. Lee, W. J. Meng, H. Yang, J. H. Han, M. Kim, Q. Y. Lu, and T. W. Noh, Ferroelectrically tunable magnetic skyrmions in ultrathin oxide heterostructures, Nat. Mater. **17**, 1087 (2018).

[22] G. Koster, L. Klein, W. Siemons, G. Rijnders, J. S. Dodge, C. B. Eom, D. H. A. Blank, and M. R. Beasley, Structure, physical properties, and applications of $SrRuO_3$ thin films, Rev. Mod. Phys. **84**, 253 (2012).

[23] J. Xia, W. Siemons, G. Koste, M. R. Beasley, and A. Kapitulnik, Critical thickness for itinerant ferromagnetism in ultrathin films of $SrRuO_3$, Phys. Rev. B **79**, 140407(R) (2009).

[24] E. M. Pugh and T. W. Lippert, Hall emf and intensity of magnetization, Phys. Rev. **42**, 709 (1932).

[25] N. Liu, J. Teng, and Y. Li, Two-component anomalous Hall effect in a magnetically doped topological insulator, Nat. Commun. **9**, 1282 (2018).

[26] A. Gerber, Interpretation of experimental evidence of the topological Hall effect, Phys. Rev. B **98**, 214440 (2018).

[27] D. Kan, T. Moriyama, K. Kobayashi, and Y. Shimakawa, Alternative to the topological interpretation of the transverse resistivity anomalies in $SrRuO_3$, Phys. Rev. B **98**, 180408(R) (2018).

[28] D. J. Groenendijk, C. Autieri, T. C. van Thiel, W. Brzezicki, N. Gauquelin, P. Barone, K. H. W. van den Bos, S. van Aert, J. Verbeeck, A. Filippetti, S. Picozzi, M. Cuoco, and A. D. Caviglia, Berry phase engineering at oxide interfaces, arXiv preprint arXiv:1810.05619 (2018).

[29] L. F. Wang, Q. Y. Feng, H. G. Lee, E. K. Ko, Q. Y. Lu, and T. W. Noh, Controllable thickness inhomogeneity and Berry-curvature-engineering of anomalous Hall effect in $SrRuO_3$ ultrathin films, arXiv preprint arXiv:1908.08211 (2019).

[30] J. He, A. Borisevich, S. V. Kalinin, S. J. Pennycook, and S. T. Pantelides, Control of Octahedral Tilts and Magnetic Properties of Perovskite Oxide Heterostructures by Substrate Symmetry, Phys. Rev. Lett. **105**, 227203 (2010).

[31] R. Aso, D. Kan, Y. Shimakawa, and H. Kurata, Atomic level observation of octahedral distortions at the perovskite oxide heterointerface, Sci. Rep. **3**, 2214 (2013).

[32] X. Liu, Y. Wang, P. V. Lukashev, J. D. Burton, and E. Y. Tsymbal, Interface dipole effect on thin film ferroelectric stability: First-principles and phenomenological modeling, Phys. Rev. B **85**, 125407 (2012).

[33] D. Yi, P. Yu, Y. C. Chen, H. H. Lee, Q. He, Y. H. Chu, and R. Ramesh, Tailoring magnetoelectric coupling in $BiFeO_3/La_{0.7}Sr_{0.3}MnO_3$ heterostructure through the interface engineering, Adv. Mater. **31**, 1806335 (2019).

[34] R. Mathieu, A. Asamitsu, H. Yamada, K. S. Takahashi, M. Kawasaki, Z. Fang, N. Nagaosa, and Y. Tokura, Scaling of

the Anomalous Hall Effect in $Sr_{1-x}Ca_xRuO_3$, Phys. Rev. Lett. **93**, 016602 (2004).

[35] G. Kresse and J. Furthmüller, Efficient iterative schemes for ab initio total-energy calculations using a plane-wave basis set, Phys. Rev. B **54**, 11169 (1996).

[36] Y. J. Shin, Y. Kim, S. J. Kang, H. H. Nahm, P. Murugavel, J. R. Kim, M. R. Cho, L. F. Wang, S. M. Yang, J. G. Yoon, J. S. Chung, M. Kim, H. Zhou, S. H. Chang, and T. W. Noh, Interface control of ferroelectricity in an $SrRuO_3/BaTiO_3/SrRuO_3$ capacitor and its critical thickness, Adv. Mater. **29**, 1602795 (2017).

[37] H. J. Chang, S. V. Kalinin, A. N. Morozovska, M. Huijben, Y. H. Chu, P. Yu, R. Ramesh, E. A. Eliseev, G. S. Svechnikov, S. J. Pennycook, and A. Y. Borisevich, Atomically resolved mapping of polarization and electric fields across ferroelectric/oxide interfaces by Z-contrast imaging, Adv. Mater. **23**, 2474 (2011).

[38] Y. M. Kim, A. Morozovska, E. Eliseev, M. P. Oxley, R. Mishra, S. M. Selbach, T. Grande, S. T. Pantelides, S. V. Kalinin, and A. Y. Borisevich, Direct observation of ferroelectric field effect and vacancy-controlled screening at the $BiFeO_3/La_xSr_{1-x}MnO_3$ interface, Nat. Mater. **13**, 1019 (2014).

[39] K. S. Takahashi, H. Ishizuka, T. Murata, Q. Y. Wang, Y. Tokura, N. Nagaosa, and M. Kawasaki, Anomalous Hall effect derived from multiple Weyl nodes in high-mobility $EuTiO_3$ films, Sci. Adv. **4**, eaar7880 (2018).